High-Resolution Patterning and Transferring of Graphene-Based Nanomaterials onto Tape toward Roll-to-Roll Production of Tape-Based Wearable Sensors

*Seval Oren, Halil Ceylan, Patrick S. Schnable, and Liang Dong**

This paper reports on a simple and versatile method for patterning and transferring graphene-based nanomaterials onto various types of tape to realize flexible microscale sensors. The method involves drop-casting a graphene film on a prepatterned polydimethylsiloxane (PDMS) surface containing negative features by graphene suspensions, applying Scotch tape to remove the excess graphene from the nonpatterned areas of the PDMS surface, and then transferring the patterned graphene from the inside of the negative features at the PDMS surface onto a target tape. The feature size of transferred graphene patterns on the final tape is as small as a few micrometers. This method is easy to implement, but does not require the use of expensive equipment, except for needing a PDMS substrate containing negative features. This method has a high versatility in producing micropatterns of graphene-based nanomaterials on different types of adhesive tape. For the purpose of application demonstration, flexible mechanical sensors and sensor arrays, smart gloves, and plant leaf sensors on tapes to realize real-time monitoring of important signals indicating human motion and plant water transport behavior have been developed. This technology will open a new route for low-cost, scalable, and roll-to-roll production of graphene-based sensors on tape.

1. Introduction

Flexible plastic substrates (e.g., polyethylene terephthalate, polyimide, and polydimethylsiloxane or PDMS)[1–6] and other nonconventional substrates (e.g., paper, tape, and cloth)[7–10] have been widely utilized as the base materials of flexible electronic devices. Conductive nanomaterials, such as carbon nanotubes, metal oxide nanowires, and graphene, have also attracted considerable attention as functional materials for applications ranging from transistors, to sensors, to energy harvesting and storage devices.[11–22] Among these conductive nanomaterials, graphene plays a key role in producing next-generation sensors owing to its unique properties, including atomic thickness, large surface area, fast electron mobility, good piezoresistivity, and high mechanical flexibility.[23–27] As a result, integrations between flexible substrate materials and graphene-based nanomaterials have led to a variety of sensors and other electronic devices through development of novel fabrication processes, advancing emerging and significant fields such as real-time motion tracking,[28] structural and human health monitoring,[29–31] electronic skin sensing,[32–36] and humanized robotic manipulation.[37] It is well known that repeated mechanical exfoliation to peel single- or few-layer graphene from bulk graphite using sticky tape and transfer it to another surface is rather uncontrollable in terms of the number of graphene layers, location, and size of the peeled graphene.[38] Recently, graphene film electrodes at centimeter scale have been fabricated by peeling tape from a commercial graphite foil for the detection of glucose,[39] but the obtained electrodes did not have well-defined shapes or control over thickness. Physically rubbed graphene electrodes have also been produced by directly placing solid-state graphene powders at a channeled adhesive surface and then rubbing against the surface.[40] The resulting graphene patterns, however, have poor feature resolution. Photolithography-based microfabrication for graphene patterning[41–49] is relatively complex and requires multiple steps such as film deposition, lithography, and etching. Recently, various interesting methods have been developed for patterning and transferring graphene-based materials onto different substrates. For example, laser printing of graphene has been studied with variable laser energy, spot size, and pulse duration.[50–54] This method, however, requires sophisticated lasers and is limited to producing patterns with minimum feature size of several tens of micrometers. An ink-jet printing

S. Oren, Prof. L. Dong
Department of Electrical and Computer Engineering
Iowa State University
Ames, IA 50011, USA
E-mail: ldong@iastate.edu
Prof. H. Ceylan
Department of Civil
Construction, and Environmental Engineering
Iowa State University
Ames, IA 50011, USA
Prof. P. S. Schnable
Department of Agronomy
Iowa State University
Ames, IA 50011, USA
Prof. P. S. Schnable
Department of Genetics
Development and Cell Biology
Iowa State University
Ames, IA 50011, USA

DOI: 10.1002/admt.201700223

method has also produced patterns of reduced graphene oxide (rGO), but resolution is poor and, for practical applications, additional laser processing is required to improve electrical conductivity of rGO.[55] A transfer printing method involves first creating graphene patterns on an initial substrate, and then utilizing a stamping process to transfer them onto a final substrate.[56] Micro transfer molding is based on filling the carved patterns of a stamp emplaced on top of a target substrate with graphene-based suspensions, followed by vacuum drying and removing the stamp from the final substrate.[57] Both the transfer printing and molding methods require a special care to modify the surface properties of the device substrates and functional materials. In addition, most existing graphene-based sensors cannot be easily installed onto the irregular surfaces of the sensed objects so, despite the efforts made, many problems remain unsolved before a large-scale, cost-effective graphene patterning method with high feature resolution and process simplicity can be realized.

In this paper, we report on a simple, high-resolution, and scalable graphene patterning and transferring method toward roll-to-roll production of flexible graphene sensors. This method involves (i) creating graphene patterns inside prepatterned negative features at the surface of a polydimethylsiloxane (PDMS) substrate using a unique "Drop cast-Dry-Stick-Peel" (D^2SP) method, and subsequently (ii) transferring the resulting graphene patterns onto a final sticky tape via an easy-to-implement "Stick-and-Transfer" (ST) process. The feature size of the transferred graphene structure on the final tape can be as small as a few micrometers. This method does not require the use of any expensive equipment, except for needing a PDMS substrate containing negative features. The versatility of this approach is demonstrated by producing complex graphene and rGO micropatterns onto different tapes commercially available (e.g., polyimide, Scotch, 3M electrically conductive, and aluminum foil adhesive tapes). Furthermore, tape-based flexible graphene pressure and strain sensors, sensor-enabled smart gloves, and plant leaf humidity sensors are realized to interact with humans and plants for real-time monitoring of important signals. We have demonstrated that smart gloves with multiple strain and pressure sensors allow real-time tracking of finger motion behavior during capturing a moving object, while graphene-based humidity sensors can be made to adhere to leaf surfaces to monitor water movement within plants upon irrigation. These sensors are flexible enough to highly conform to various irregular shapes of the sensed objects. The patterning and transferring method presented outperforms many other counterpart approaches in terms of pattern spatial resolution, thickness control, process simplicity, and diversity with respect to functional materials and pattern geometries.

The main procedures for forming graphene patterns on the tape surface are illustrated in **Figure 1**. Briefly, a master Si mold with positive patterns made of SU-8 photoresist was first formed on the surface of a silicon wafer, and negative patterns were then formed on a PDMS substrate from the Si mold via soft lithography (Figure 1a). Here, the "negative" patterns or features refer to the "channels" or cut out areas at the PDMS surface. Subsequently, aqueous suspensions of graphene nanoplatelets were loaded onto the PDMS surface (Figure 1b). After drying on a hotplate in air, a thin graphene film was formed, covering the entire PDMS surface (Figure 1c). Next, Scotch tape was manually applied and stick to the top surface, and then peeled the excess graphene from the nonpatterned areas on the surface. This stick-and-peel process was repeated to ensure complete removal of the unwanted graphene from the top surface (Figure 1d), while the graphene inside the PDMS negative patterns remained intact because it was set below the top surface. Therefore, the D^2SP process was completed, resulting in the graphene structures inside the negative patterns on the PDMS surface (Figure 1e). After that, transfer of the formed graphene patterns onto a final target tape was implemented by manually applying and pressing the target tape, and then peeling it from the PDMS surface (Figure 1f,g). The ST process was thus completed and the microscale graphene patterns were formed onto the surface of the final tape. Figure 1h–l displays the images for the main procedures of the D^2SP and ST processes. The details of fabrication are described in the Experimental Section. A video showing the process to obtain the graphene patterns on the tape surface is given in the Supporting Information.

Essentially, the tape-based graphene patterning and transfer technique utilizes the work of adhesion $W_{A\text{-}B}$ at the interface between two contacting materials A and B as determined by their surface energies,[59,60] with $W_{A\text{-}B}$ given by[61]

$$W_{A\text{-}B} = 4\left(\frac{\gamma_A^d \gamma_B^d}{\gamma_A^d + \gamma_B^d} + \frac{\gamma_A^p \gamma_B^p}{\gamma_A^p + \gamma_B^p}\right) \quad (1)$$

where γ^d and γ^p correspond to the dispersion and polar components of surface energy ($\gamma = \gamma^d + \gamma^p$). Table S1 (Supporting Information) provides the surface energies of the materials used in this work[68–70] and the calculated values of $W_{graphene\text{-}PDMS}$ at the interfaces between graphene and PDMS and $W_{graphene\text{-}tape}$ between graphene and tape. The fact that $W_{graphene\text{-}tape} > W_{graphene\text{-}PDMS}$ for different types of tape makes it possible to remove the excess graphene from the PDMS top surface using the cleaning Scotch tape during the D^2SP process, and transfer the patterned graphene onto the target tape during the ST process. See the Supporting Information for the values of $W_{A\text{-}B}$ for different material combinations.

2. Results and Discussion

2.1. Microscale Patterning and Transferring

Figure 2 shows several examples of microscale graphene patterns transferred onto a 25 μm thick polyimide tape with silicone adhesive. The PDMS substrate used here contained 15.4 μm deep negative features prefabricated at its surface. The graphene structures inside these negative patterns were 10.3 ± 2.7 μm thick, which was determined by a surface profilometer (see the measurement method in the Experimental Section). The transferred patterns were of high spatial resolution (≈5 μm), and mostly retained the features of the original patterns at the PDMS surface. This method also allowed producing graphene patterns on a tape roll, as shown in Figure 2f–h (see Figure S1, Supporting Information, for the fabrication process). It should be noted that, to realize these

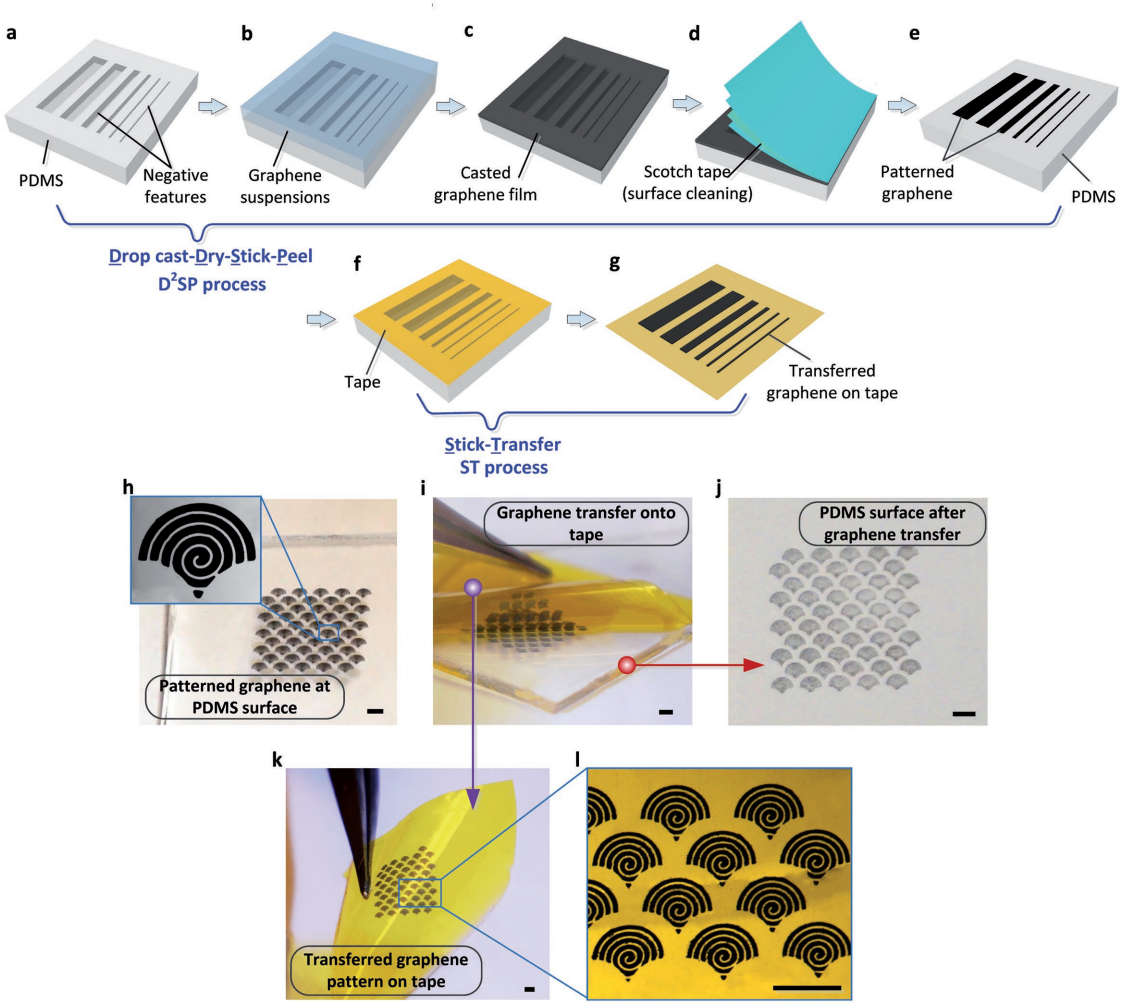

Figure 1. a–g) A schematic representation of the graphene pattern formation on tape. a) Negative patterns created on the PDMS substrate via soft lithography. b) Graphene suspensions drop-coated onto the entire surface of the PDMS slab. c) A graphene film formed on the PDMS surface. d) The graphene film outside the negative patterns removed using Scotch tape. e) Graphene patterns formed inside the negative patterns at the PDMS surface. f) A target tape adhered onto the PDMS surface. g) Graphene patterns transferred onto the target tape. h,i) Optical images showing the main steps of graphene patterning and transferring process. The scale bars represent 1 mm. h) Graphene patterns obtained in the PDMS structures. The negative patterns on the PDMS substrate were 15.4 µm deep. The graphene inside the PDMS negative patterns were 10.3 µm thick. i) Application of the ST process for graphene pattern transfer onto the polyimide tape. j) PDMS surface after graphene transfer. k,i) Graphene patterns transferred onto the polyimide tape.

graphene patterns on a tape, several critical geometrical and processing parameters, including the volume of graphene suspensions over the unit surface area, the depth, and width of the preformed negative features at the PDMS surface, and the number of repeating D^{2}SP times, should be carefully considered. The following section will discuss the influences of these parameters on the quality of pattern formation and transfer.

First, although a thick graphene film could easily be produced by loading a large volume of graphene suspensions per unit surface area onto the PDMS surface, patterning of a thick film was difficult using the D^{2}SP method. The experiment here utilized a PDMS substrate containing 15.4 µm deep and 500 µm wide channels at its surface, and was covered by a 10.3 µm thick graphene film. This thick film was formed by drop-casting with 20 mg mL^{-1} concentration graphene suspensions at a large volume per unit surface area of 710 µL cm^{-2} (**Figure 3**a, top). Then, Scotch tape was applied and stick to the PDMS surface, with an intent to clean the PDMS surface by removing the unwanted graphene from the PDMS top surface. However, as shown schematically in Figure 3a and experimentally in Figure 3b, some portions of the graphene inside the channels were also removed by the Scotch cleaning tape. A possible explanation for this is that the tape peeling could not easily break such a thick graphene film at the step and sidewall of the channel completely covered by the continuous graphene film. Therefore, to successfully produce thick graphene patterns in the PDMS channels, sequential D^{2}SP processes were applied multiple times (each time producing a thin film until the desired film thickness was achieved (Figure 3c). Specifically, our experiment shows that when the drop-casted graphene film was no more than ≈1.5 µm thick, Scotch tape worked perfectly to break the film at the step of the channel, almost regardless of

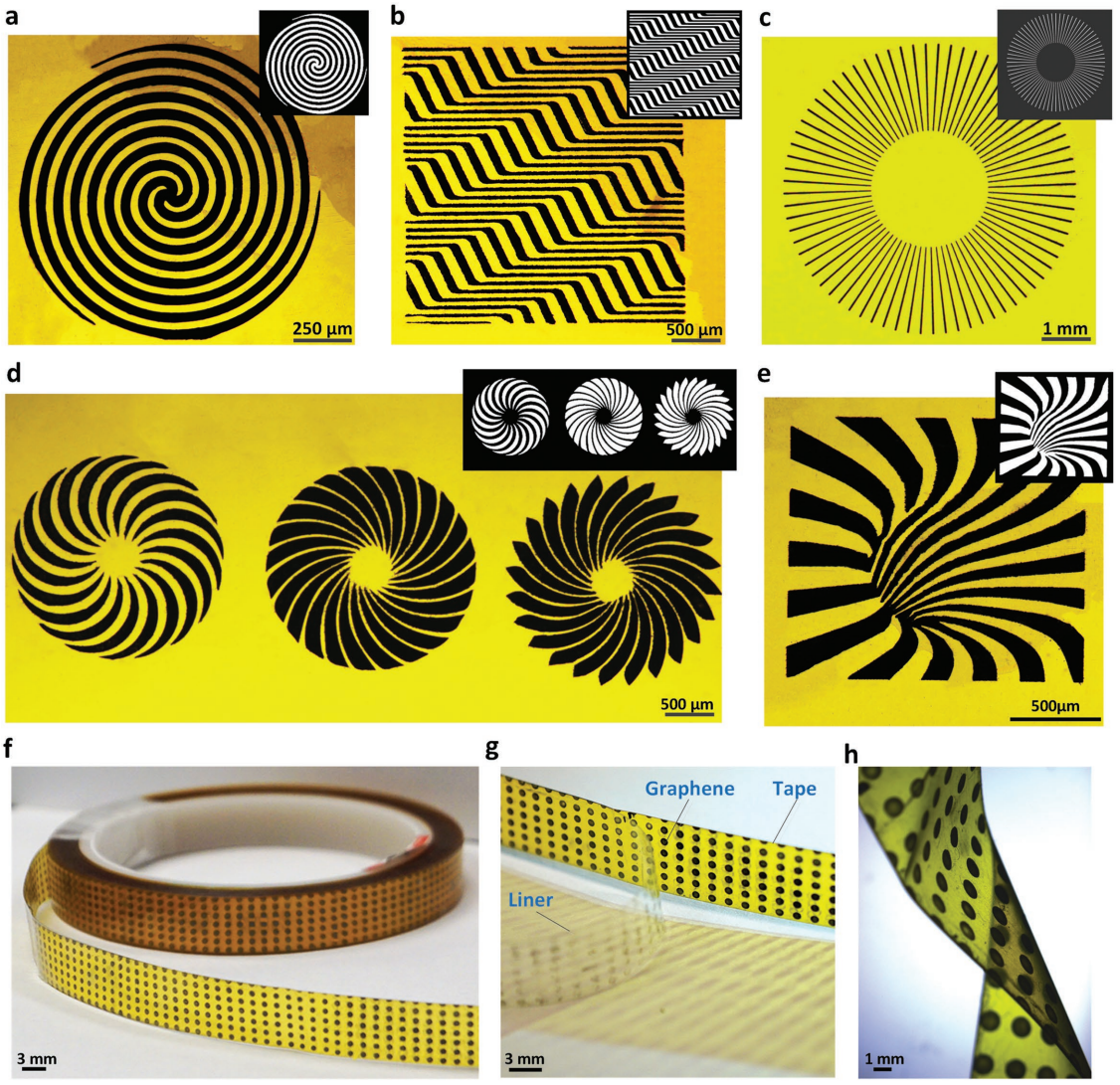

Figure 2. a–e) Versatile graphene patterns formed on the polyimide tape using the proposed method. f–h) Formation of graphene patterns on the relatively large polyimide tape roll with liner. The transferred graphene patterns are protected by a nonsticky liner.

the channel depth, as long as the tape was not in direct contact with the graphene inside the channel. Therefore, in the subsequent experiments, graphene suspensions (concentration: 20 mg mL^{-1}) were loaded to the PDMS surface (the volume of graphene suspensions per unit surface area: 100 μL cm^{-2}) to form an ≈1.45 μm thick graphene film (Figure 3c, top). Next, this thin film was patterned to form the graphene structures inside the channel using the stick-and-peel process with Scotch tape (Figure 3c, middle). To increase the thickness of the graphene patterns inside the channel, the whole D^2SP process (described in Figure 1a–e) was repeated multiple times until a desired thickness was obtained (Figure 3c, bottom). Figure 3d shows the PDMS channel filled by an ≈10.3 μm thick graphene film after seven times repeated D^2SP processes. Figure 3e shows the optical images for the graphene patterns in the PDMS channels obtained with 1–7 times repeated D^2SP processes. Figure 3f shows that the graphene patterns exhibit a linear increase in thickness and a linear decrease in electrical resistance with the number of repeated D^2SP processes (or the number of coatings).

Next, to transfer the patterned graphene from the PDMS channels onto a final tape via the ST process, we investigated the influences of the channel width and depth on the transfer quality. The experiment here utilized the PDMS channels with depths of 5, 15.4, and 41.6 μm, and widths of 20, 40, and 100 μm. By performing sequential D^2SP processes, the channels were almost fully filled by graphene, with a few micrometers gap distance to the channel top. Polyimide tapes with silicone adhesive were used to transfer the graphene patterns, with results indicating that, after the graphene structures were transferred onto the tape, the 41.6 μm deep channels of all the different widths contained graphene residues as shown in Figure 3g. This may be because the van der Waals force within the drop-casted graphene film was not large enough to hold the ≈36.7 μm thick graphene structure together during transferring using the tape. The other plausible cause may be due

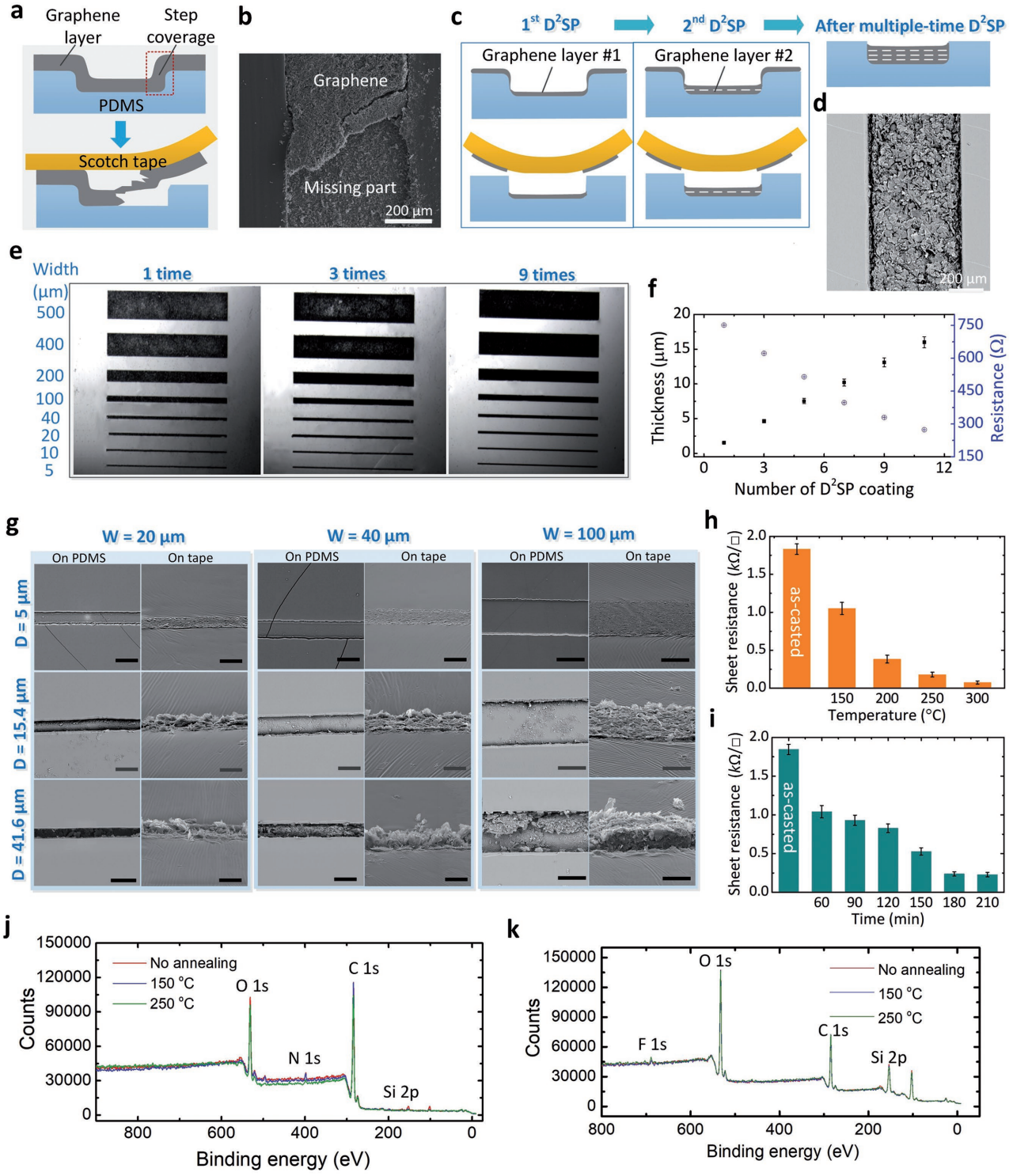

Figure 3. a) A schematic representation of forming a thick graphene film over the entire PDMS surface by one time drop-casting, followed by using Scotch cleaning tape to remove the unwanted graphene from outside the patterned areas. b) SEM image of the PDMS channel containing the incomplete graphene pattern. c) A schematic representation of forming a thick graphene film over the entire PDMS surface via multitime D^{2}SP processes. d) SEM images of the PDMS channel filled with the complete graphene pattern after multiple D^{2}SP processes were applied. e) Optical images for three groups of graphene patterns inside the PDMS channels. The numbers "5–500 μm" and "1–3–7" represent PDMS channel widths, and numbers of graphene layers formed inside the PDMS channel by repeated D^{2}SP processes, respectively. f) Thickness and electrical resistance of the graphene filled in the PDMS channel as a function of the number of D^{2}SP coatings. Each coating here is 1.45 ± 0.32 μm thick. g) Analysis of influences of channel width and depth on the transfer process. The magnitudes of 20, 40, and 100 μm represent the channel widths, while the values of 5, 15.4, and 41.6 μm denote the channel depths. The scale bars represent 50 μm. Sheet resistance of transferred graphene patterns (≈10.3 μm thickness) on the polyimide

to an increased drag force occurring at the large-area sidewalls of the deep channel and acting on the graphene during peeling. When the channel depth decreased to 15.4 μm and contained ≈10.3 μm-thick graphene, the tape transfers of graphene became easier and only a very minor residue remained in the channels. With decreasing channel width from 100 to 20 μm, the increased aspect ratio of the channel led to somewhat increased amounts of residue at the channel edges, but overall the transferred graphene on the tape retained the original pattern features of the graphene structures in the channels. Furthermore, in the case of transferring ≈2.3 μm thick graphene from the 5 μm deep channels, no residues were observed to remain in the channels for all widths.

To increase electrical conductivity of the transferred graphene, the transferred graphene patterns on the polyimide tape were annealed in air. Essentially, thermal treatment may improve contacts between graphene nanoplatelets, and thus increase electrical conductance of the formed graphene patterns.[58] Because polyimide tapes are dimensionally stable below 400 °C,[62] the annealing was carried out at temperatures ranging from 150 to 300 °C (Figure 3h) over different treating times ranging from 60 to 210 min (Figure 3i). The results show that the sheet resistance of the transferred graphene (≈10.3 μm thickness) was decreased by about seven times after the treatment at 250 °C for 180 min. Increased annealing time did not help to further decrease the sheet resistance. As the annealing temperature increased toward 300 °C, the sheet resistance was found to decrease, but, the optimum annealing temperature was chosen as 250 °C because of the above-mentioned critical temperature restriction of polyimide tape.[62]

X-ray photoelectron spectroscopy (XPS) was used to characterize the composition of the transferred graphene structures on tape before and after thermal treatment. Figure 3j,k depicts the XPS survey spectra for two groups of samples, that is, the transferred graphene (thickness: ≈10.3 μm) on a 25 μm thick polyimide tape, and the polyimide tape alone. There were three samples in each group, including one treated at 150 °C for 180 min, one 250 °C for the same time, and another not treated. The results show that all the on-tape graphene samples contain peaks assigned to C 1s (284 eV), O 1s (531.3 eV), N 1s (398.6 eV), and Si 2p (101.4 eV) (Figure 3j), and all the polyimide tape samples exhibited peaks belongs to C 1s (284.6 eV), O 1s (532.7 eV), F 1s (688.6 eV), and Si 2p (102.4 eV) (Figure 3k). For the on-tape graphene samples, O 1s peak occurs due to the physically adsorbed oxygen;[63] Si 2p peak might originate from the adhesive of the polyimide tape; and N 1s peak was observed because the graphene used here is N-doped graphene nanoplatelets.[64] Further, high-resolution spectra analysis (Figures S2 and S3, Supporting Information) confirms that the thermal treatment did not make distinct changes to the chemical structure of the graphene and polyimide tape samples, although the intensity of C 1s peak decreased slightly at 250 °C. The intensity of Si 2p peak of the graphene pattern decreased as the temperature increased up to 250 °C (Figure S2c, Supporting Information).

The present patterning and transferring method could also be employed to obtain rGO patterns on tape. **Figure 4**a shows some rGO strip patterns formed inside the PDMS channels at different coating (or D^2SP) times, and Figure 4c–e shows the rGO patterns transferred onto the polyimide tape, using essentially the same method as described in Figure 1. The film thickness of the rGO linearly increased with coating time (Figure 4b). The experiments here utilized a PDMS substrate with 15.4 μm deep negative features at its surface. Five repeated D^2SP processes were sequentially applied to obtain the rGO patterns inside the negative features. For each coating, 100 μL cm^{-2} of rGO suspensions (20 mg mL^{-1} in the mixture of ethanol and DI water at a volume ratio of 7:3) were drop-coated over the entire PDMS surface.

In addition, the present method can also be used to produce graphene patterns on different adhesive substrates such as Scotch and aluminum foil tapes, both with acrylic adhesive (Figure 4f,g), and Scotch tape with synthetic rubber adhesive (Figure 4h). All the graphene patterns in Figure 4f–h were formed with five repeated D^2SP times and transferred onto the target tapes with the ST process.

2.2. Application Demonstrations

2.2.1. On-Tape Strain Sensors

A graphene strip pattern (6 mm length, 800 μm width, and 10.3 μm thickness) was transferred onto the polyimide tape as a strain sensor. The sheet resistance of the patterned graphene was 0.22 ± 0.12 kΩ sq^{-1}. Electrical contacts between the graphene pattern and external tin copper electronic wires (Gauge 20) were realized with silver paste. **Figure 5**a shows the resistance response of the sensor to a tensile strain applied along the length direction of the graphene pattern. The relative resistance changes of the sensor ($\Delta R/R$) increased linearly with applied tensile strain. The gauge factor of the sensor was found to be 12.16 from the slope of the linear fitting curve in Figure 5a. Figure 5b,c demonstrated the stability of the sensor by loading and unloading a 4.4% tensile strain for 100 times. The hysteretic behavior of the sensor was also investigated. The sensor was stretched up to 6% strain at the rate of 1.2% s^{-1}, and then released back to the initial position at the same rate (Figure 5d), exhibiting a low hysteretic behavior, which may be attributed to the elastic deformation of the sensor materials.[65] When the sensor was attached to the surface of a growing balloon, the value of $\Delta R/R$ increased due to the stretching of the graphene strip (Figure 5e). When the balloon was in a temporarily static state, the sensor resistance remained constant. The tape-based strain sensor

tape at different h) annealing temperatures and i) durations (i). XPS survey spectra for graphene patterns transferred onto j) polyimide tapes and k) the polyimide tape alone, without thermal treatment and annealed at 150 and 250 °C for 180 min. The error bars in (f), (h), and (i) represent standard deviations of three independent experiments using three samples.

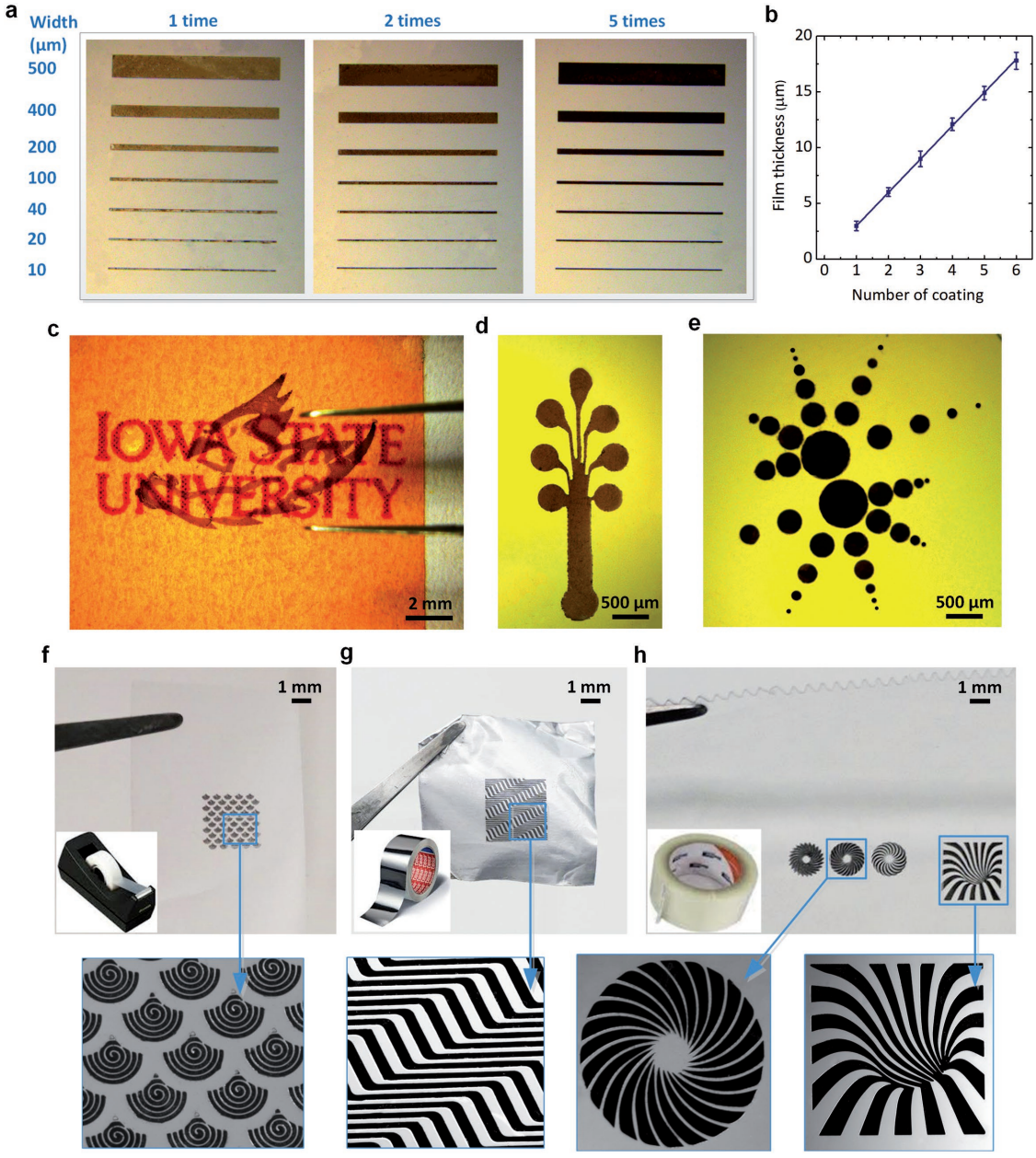

Figure 4. a) Optical images of the rGO patterns inside the PDMS channels with a channel depth of 15.4 μm. The numbers "10–500 μm" and "1–2–4" denote the channel widths and numbers of graphene layers inside the PDMS channels, respectively. b) Thickness of the GO patterns measured at different D^2SP times. The error bars represent standard deviations of three independent experiments using three samples. Various rGO patterns obtained on the polyimide tapes using a c) one-time, d) two-time, and e) five-time D^2SP repeated process, followed by the ST process. Optical images of the graphene patterns fabricated on various tape substrates, including f) Scotch tape with acrylic adhesive, g) aluminum foil tape, and h) Scotch tape with synthetic rubber adhesive.

was therefore capable of monitoring strain variations at an object's surface.

In another test, the same type of sensor was attached to the middle joint of an index finger to measure the tensile strain formed during finger bending (Figure 5f). As the degree of bending increased from 5° to 90°, the value of $\Delta R/R$ of the sensor increased from 33.8 to 147.5%. After the finger returned to its original position, the sensor resistance immediately resumed its initial value, demonstrating good reversibility of the sensor response.

2.2.2. On-Tape Pressure Sensors

The above-mentioned strain sensor was adopted as an on-tape pressure sensor in this demonstration. **Figure 6**a shows that the $\Delta R/R$ value produced by the sensor increased with increasing pressure applied normal to the surface of the sensor. Based on the slopes of the linear fitting curves in different pressure ranges, the sensitivity of the sensor was found to be $S = 0.13\ \text{kPa}^{-1}$ for applied pressures below 300 kPa, and

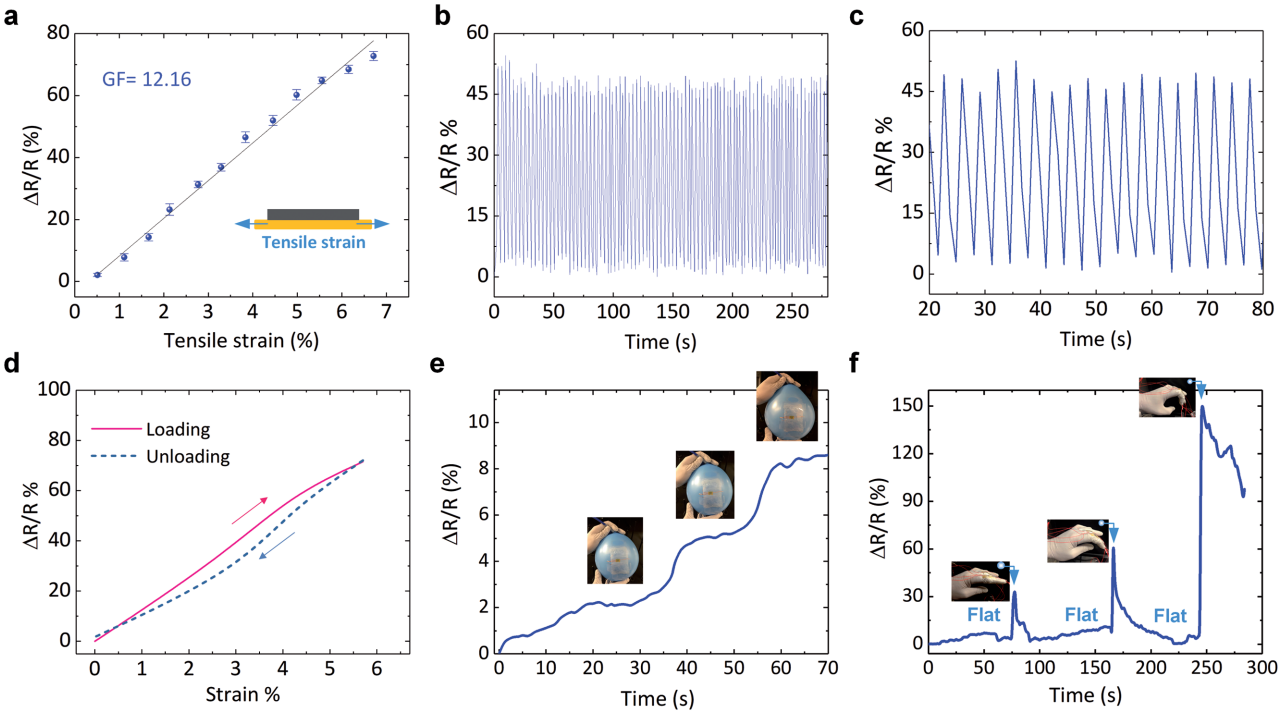

Figure 5. Demonstration of using a transferred graphene pattern as a strain sensor. a) Relative change in resistance as a function of the tensile strain applied along the length direction of the graphene pattern. The error bars represent standard deviations of three independent experiments using three sensors and demonstrate good reproducibility of the sensors. b) Relative resistance of the sensor with the repetition of 100 loading/unloading cycles by 4.4% strain. c) Enlarged view of (b), exhibits a stable sensor performance. d) Hysteresis curve of the strain sensor. e) Monitoring of tension changes on the balloon surface during inflation. f) Monitoring of bending motions of the index finger.

$S = 0.053$ kPa^{-1} in a higher pressure range up to 575 kPa. To verify durability of the sensor, the device was loaded (pressure normal to the sensor surface: 330 kPa) and unloaded for 100 cycles. No obvious degradation of the sensor response was observed after the testing (Figure 6b,c). In addition, the sensor exhibited a response time of ≈0.3 s (Figure 6d).

This sensor was used to measure the pulse in the wrist. Figure 6e shows that the wrist pulses, 75 beats min^{-1}, were counted via the time-varying relative resistance changes. Next, the sensor monitored repetitive finger clicking of a computer mouse. When the mouse was clicked, the $\Delta R/R$ value of the interacting sensor increased. Figure 6f demonstrates that the sensor continuously tracked various clicking pressures and frequencies.

As another example application, an array of 10 × 10 round-shaped graphene sensors was formed on 3M electrically conductive tape (Conductive adhesive transfer tape 9707) (Figure 6g). Each sensing element had a diameter of 1 mm, a thickness of ≈10.3 µm, and a pitch of 1.5 mm. Because this type of tape could sustain temperatures up to 85 °C,[66] the transferred graphene was further annealed in air at 80 °C for 4 h to reduce its sheet resistance to 4.05 ± 0.18 kΩ sq^{-1}. These sensing elements were connected to an external detection circuit through an array of 10 × 10 vertical pogo pins (No. 575-09510152071, Mouser Electronics) formed on a printed circuit board and arranged in the same manner as the sensing elements (Figure 6g). The conductive tape served as a common ground for the sensing elements. To facilitate pressure application to the sensor array, the tape and pogo pins were embedded in a PDMS layer. After applying external pressure, changes in resistance were recorded by a multimeter through a multiplexer. Figure 6h shows that when a finger was pressed or a key was positioned on the surface of the device, the embedded sensor array could monitor its interaction with the object and identify the shape and pressure (or resistance) profile of the object.

2.2.3. Smart Glove

Figure 7 depicts a smart glove equipped with on-tape strain and pressure sensors for monitoring mechanical response of fingers when interacting with an object. Specifically, each finger was equipped with a pressure sensor at its fingertip and a strain sensor at the top of the finger joint, respectively (Figure 7b,c). These sensors enabled real-time monitoring of changes in important mechanical parameters due to hand movements. As an example, the glove was worn while catching a tennis ball bounced from a hard floor (Figure 7d). The pressure (Figure 7e) and strain (Figure 7f) variations during preparing, adjusting, catching, and holding were obtained by the smart glove. As the ball bounded upward, the fingers adjusted to bend more, increasing the tension on the sensors. When the ball was about to reach the palm, the fingers acted to catch the ball, producing immediate increases in the applied pressure. The flexibility of these tape-based graphene sensors allowed for conformable

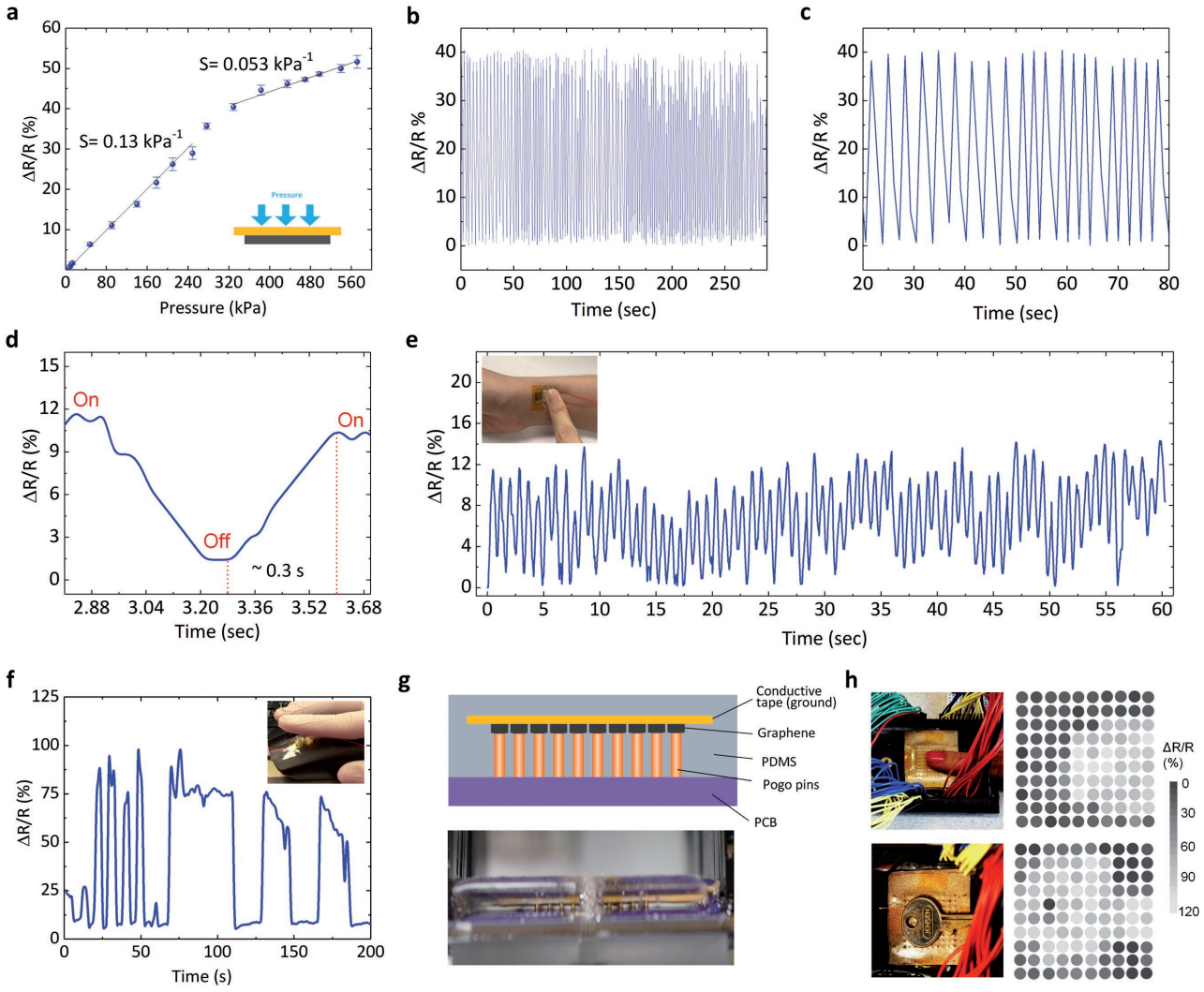

Figure 6. Demonstration of using transferred graphene pattern as a pressure sensor. a) Relative change in resistance as a function of pressure uniformly applied to the polyimide tape surface. The error bars represent standard deviations of three independent experiments using three sensors and demonstrate good reproducibility of the sensors. b) Relative resistance changes of the sensor with repetition of 100 loading/unloading cycles by 330 kPa. c) Enlarged view of (b), exhibiting a stable sensor performance. d) Response curve of the sensor with an applied pressure of 80 kPa at a response time of 0.3 s. e) Monitoring of the pulse rate of human wrist. f) Monitoring of the frequency of mouse clicking. g) Cross-sectional view of an array of 10 × 10 round-shaped graphene sensors for a pressure-mapping application. Top: schematic representation; bottom: fabricated device. h) Top view of a finger (top) and a key (bottom) positioned on the surface of the pressure sensor array and $\Delta R/R$ mapping of the pressure distributions.

contact with the fingers. Such a smart glove would be useful in measuring hand mechanical function and control in many applications, such as providing real-time data streams for medical rehabilitation therapies and human–computer interaction.

2.2.4. On-Tape Plant Leaf Sensors

Water uptake by roots, transport through the xylem, and transpiration from the stomata of leaves to the atmosphere are an important physiological process in plants. Using tape-based graphene RH sensors, we demonstrated a unique capability to estimate the time required for water movement within a plant from the roots to the lower and upper leaves (**Figure 8**a). When the stomata are open, water vapor escapes from the leaves, increasing the local humidity level on the leaf surface (Figure 8b). Consequently, by installing multiple RH sensors on different leaves to dynamically monitor RH variation at the leaf surfaces, it is possible to track the key time points at which significant water loss occurs at the leaves, thus quantifying water transport time via the xylem from the roots to each of the measured leaves. The RH sensors were structured as graphene strips (6 mm length, 800 µm width, and 10.3 µm thickness) transferred onto the polyimide tape, and are the same as those used in the above-mentioned pressure and strain sensing applications. The sensing mechanism is based on changes in the electrical resistance of graphene in different moisture environments. Figure 8c shows the resistance response of the fabricated sensor exposed to different RH levels at room temperature. To facilitate the installation of the sensor onto

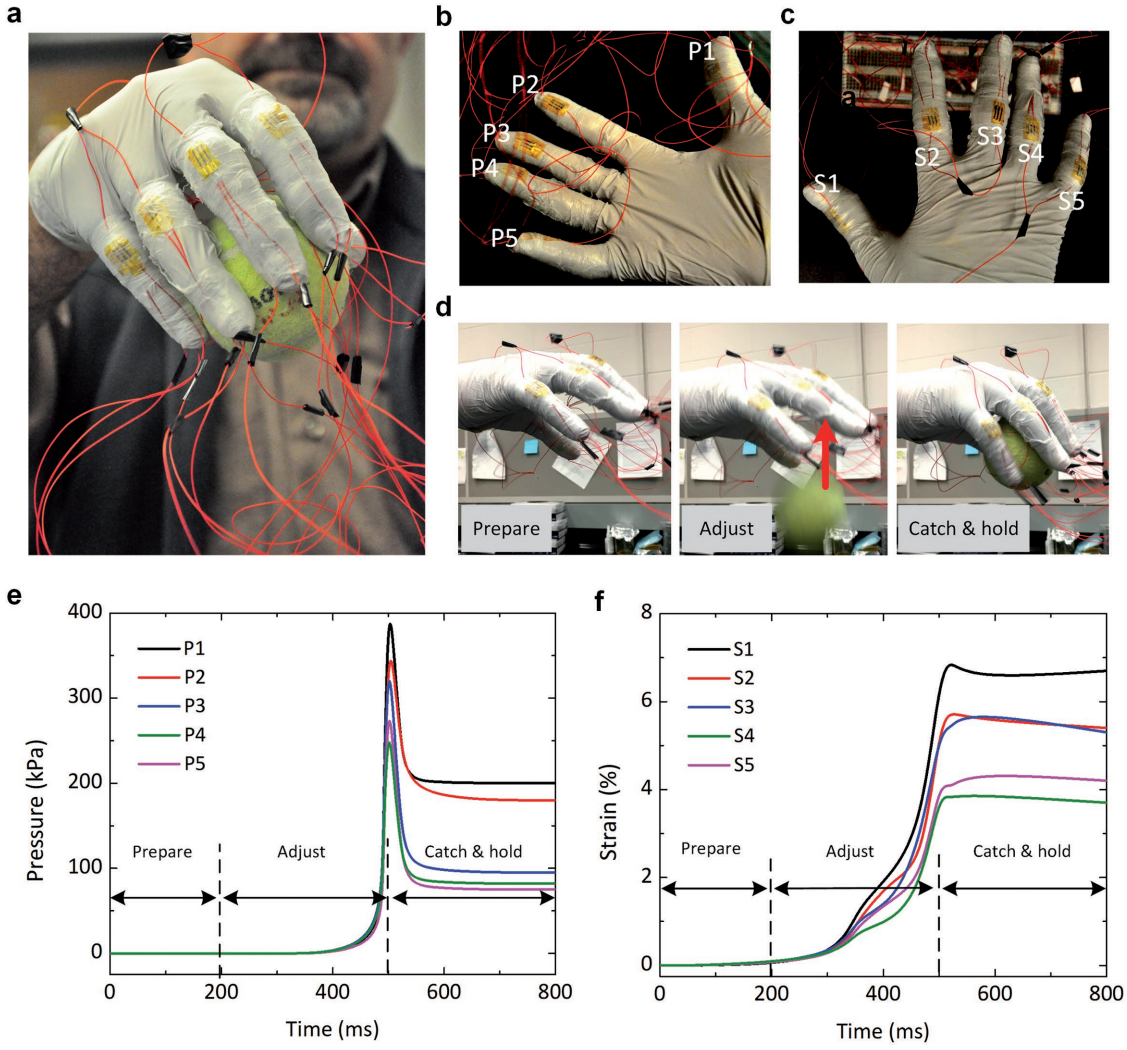

Figure 7. Demonstration of using a smart glove to monitor the pressure and strain levels during catching a tennis ball. a) An optical image of the graphene sensors attached to the finger joints. b,c) Positions of the five pressure sensors (P1–P5) and five strain sensors (S1–S5). d) Time-lapse images of catching the tennis ball using the smart glove. The three images represent the three states: preparation (left), adjustment (middle), and catching (right). Responses of the smart glove during catching the tennis ball, including e) pressure and f) strain responses.

the leaf surface, two additional tape strips (acrylic adhesive; No. 6915001 from Gorilla) were adhered to the two sides of the graphene pattern (see the inset of Figure 8c). This also created a 170 µm thick air gap between the sensor surface and the leaf, as well as two side openings that allow air exchange between inside and outside of the gap space for avoiding accumulation of water vapor. The air gap was determined by the thickness of the additional tape strips. Figure 8d,e describes real-time monitoring of RH using the sensors installed on the back surfaces of the fourth and ninth leaf of two-month old maize plants. Here, one type of plant (Figure 8d) was inbred line B73.[67] The other type (Figure 8e) was a mixed genetic stock (having a more complicated pedigree in which the female parent was a hybrid with no close relationship to B73, and the male parent was in a B73 background; they were grown in Dr. Patrick Schnable's lab at Iowa State University). The testing was initiated 15 min before irrigation. After irrigation, for B73, the lower and upper sensors exhibited a resistance increment and thus an increase in RH at 55 and 135 min, respectively. Similarly, for the mixed genetic stock, the sensor outputs of the show that the lower and upper leaves had an increase in RH at 82 and 110 min, respectively. Therefore, in both the B73 plants and plants with mixed genetic backgrounds, it took less time for water to be transported from the roots to the fourth leaf than from the roots to the ninth leaf. Significantly, these two genetic stocks exhibited differences in the delta between the fourth and ninth leaves (80 ± 11 min, mean ± standard deviation obtained from the measurements on three plants for B73 versus 28 ± 10 min, mean ± standard deviation obtained from the measurements on three plants for the plants with a mixed genetic background). Because water transport is a critical process for plants, the on-tape RH sensor technology would be useful to select plants with a desirable water transport character or improved tolerance to increasing water stress, a major objective of crop breeding.

The above demonstrations provide only a few application examples of using tape-based flexible sensors, and many other

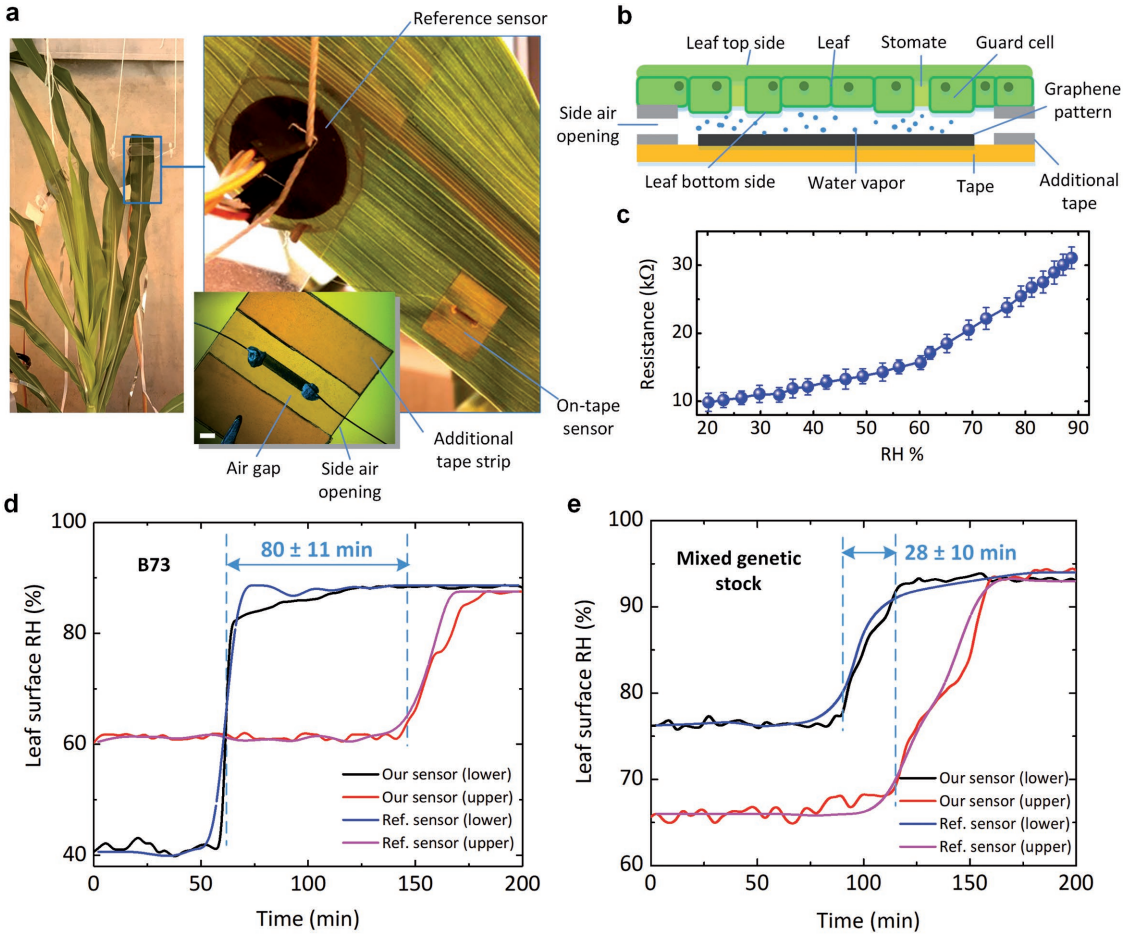

Figure 8. Demonstration of using the on-tape RH graphene sensors for the estimation of the times required for water movement within the plant from the roots to the lower and upper leaves. a) A photo of the graphene RH sensor and a commercial RH reference sensor located at the back of the maze leaf. The placement of the two sensors is magnified in the right-hand image to clarify the structure. The scale bar represents 1 mm. b) A schematic illustration of the sensor placement and detection mechanism. c) Resistance of the graphene sensor as a function of RH. The resistance is measured using a RLC meter at 100 Hz operation frequency. The error bars represent standard deviations of three independent experiments using three sensors and demonstrate good reproducibility of the sensors. d,e) Real-time monitoring of the RH level on the leaf surface after plant irrigation at two maize plants: d) B73 and e) a mixed genetic stock.

graphene sensors could be designed and manufactured on tape for use in a variety of emerging applications. For example, the graphene pressure and strain sensors could be fastened to the surfaces of mechanical and infrastructure systems for structural health monitoring purposes. By functionalizing the patterns of graphene-based nanomaterials on the tape with an enzyme substrate or a receptor ligand that respond to a specific receptor or enzyme, or by transferring materials already functionalized inside the PDMS negative features onto a tape, it would be possible to develop many wearable and disposable biological and chemical sensors on tape for applications in biomedical diagnostics (e.g., sweat glucose and electrolyte sensing), environmental monitoring (e.g., gas sensing), and agricultural monitoring (e.g., nutrient and pesticide sensing). In addition, this fabrication approach allows formation of high-resolution patterns on the surfaces of versatile tapes as long as their free surface energies are different enough to enable strong adhesion to one another. This advantage, in conjunction with the ability to control the patterns along three dimensions with high spatial resolution, would further extend the application potential of this method. Further work will aim at using the presented technology to develop on-tape sensors with different nanomaterials. We believe that this technology will open a new route for low-cost, scalable, and roll-to-roll production of various types of nanomaterials-based sensors.

3. Conclusion

In summary, a novel tape-based graphene patterning and transfer approach has been developed. It is simple and effective, and has potential to support realization of roll-to-roll production of various graphene sensors. Once PDMS negative patterns are formed via conventional soft lithography, only adhesive tapes are required to produce graphene patterns with feature resolution of a few micrometers. The method can be applied to many tapes to realize various flexible sensors, such as the demonstrated wearable graphene-based sensors for

mechanical and RH sensing on surfaces of humans and crop plants.

4. Experimental Section

Graphene Suspension Preparation: Dispersion of graphene nanoplatelets in *n*-butyl acetate (total graphene content: 23 wt%; SKU: UHC-NPD; Graphene Supermarket, Calverton, NY) was heated on a hotplate at 85 °C until it all became dried due to evaporation of the solvent from it. The average thickness of graphene nanoplatelets is ≈7 nm.[71] Subsequently, aqueous suspensions of graphene nanoplatelets (20 mg mL^{-1}) were prepared by thoroughly dispersing 20 mg of the obtained graphene nanoplatelet powder in 1 mL of a mixed solution of ethanol and deionized water at a ratio of 7:3 (vol/vol), followed by sonication at room temperature for 400 min. Here, 20 mg mL^{-1} concentration of the obtained graphene dispersions was chosen because it allowed easy spreading of the solution, while forming a continuous film over the PDMS surface. In addition, the specific 7:3 (vol/vol) ethanol-to-water volume ratio was chosen to allow sufficient dispersion and maximum concentration of graphene[58] (see the graphene dispersions prepared at different volume ratios in Figure S3, Supporting Information).

PDMS Substrate Fabrication: The PDMS negative patterns used here were fabricated using soft lithography. In this step, a silicon wafer with photoresist SU-8 (3050; MicroChem, Westborough, MA) was spin-coated to produce different thicknesses by adjusting rotation speed and duration. The wafer was then baked at 65 °C for 5 min and 90 °C for 1 h. Subsequently, the wafer was exposed to an ultraviolet light with photomask, baked at 90 °C for 30 min, and developed to form a master mold for the microfluidic channels. Following that, a precursor solution of PDMS was prepared by mixing Sylgard 184 Silicone Elastomer base and curing agent (Dow Corning, Auburn, MI) at a weight ratio of 10:1, and then degassed in a vacuum desiccator for 20 min. Finally, it was poured on the master mold and thermally cured at 65 °C for 2 h on a hotplate. Finally, the cured PDMS containing negative patterns were peeled from the master mold.

D^2SP and ST Processes: The D^2SP process was used to pattern graphene structures in the negative features on the PDMS substrate (Figure 1a–e). First, the PDMS substrate was horizontally placed on a hotplate. A 3 mm high, 50 mm diameter acrylic plastic ring was then placed on the edges of the PDMS substrate to confine graphene dispersions on the substrate surface. Next, the graphene dispersions (20 mg mL^{-1}) were loaded into the plastic ring using a medical syringe. The volume of graphene dispersions per unit surface area was 100 µL cm^{-2}. The loaded graphene solution was then heated on the hotplate at 90 °C for 5 min, thus forming a casted graphene film. Subsequently, Scotch tape with synthetic rubber adhesive (Scotch Heavy Duty Shipping Packaging Tape) was manually applied and stick to the PDMS top surface. As the tape was then peeled, the graphene in the nonpatterned areas was removed from the PDMS surface. The D^2SP process was repeated multiple times until the PDMS top surface was cleaned. Therefore, the graphene patterns (thickness: ≈1.45 µm) were obtained in the negative features on the PDMS surface, without any residues left on the nonpatterned areas. To increase the thickness of graphene patterns, the D^2SP process was repeated. For example, to obtain ≈10.3 µm thick graphene patterns, one needs to repeat the D^2SP process for seven times.

Next, the ST process was conducted to transfer the formed graphene patterns from the PDMS surface onto a final tape. In this step, the final tape was applied and stick to the PDMS surface. A minor pressure was applied to achieve a conformal contact between the tape and the graphene flakes filled in the negative surface features. Subsequently, the tape was manually peeled from the PDMS substrate, and thus the graphene patterns were stick and transferred onto the surface of the tape.

To increase electrical conductivity of the transferred graphene patterns, thermal annealing was conducted at 250 °C for 180 min in air (Thermolyne Benchtop Muffle Furnace; Thermo Scientific, Waltham, MA).

X-Ray Photoelectron Spectroscopy Analysis: The XPS measurements were performed using a PHI ESCA 5500 instrument (Perkin-Elmer Co., MN). Each sample was irradiated with 200 W unmonochromated Al Kα X-rays. The pass energy was set at 188 eV for survey scans and 47 eV for narrow scans.

Thickness Measurement for Graphene Patterns in PDMS Channel: The thickness of graphene formed in the PDMS channel was measured using a surface profilometer (XP-100; Ambios Technology, Santa Cruz, CA). First, the profilometer was used to measure the surface profile and depth (H_1) of the PDMS channel. After the D^2SP process was completed, the graphene structures were formed in the channel. The profilometer was then used to determine the new depth (H_2) of the channel filled with graphene. Therefore, the thickness of the graphene patterns was calculated as H_1–H_2. In this study, informed and signed consent was obtained from the participants of the experiments performed on human subjects.

Supporting information

Supporting Information is available from the Wiley Online Library or from the author.

Acknowledgements

This work was supported in part by the Iowa Department of Transportation, the Iowa Highway Research Board, the Plant Sciences Institute at Iowa State University through the PSI Faculty Scholar program, and the U.S. National Science Foundation under Grant No. DBI-1353819. S.O. thanks the Turkish Council of High Education and Anadolu University, Turkey, for partial financial support. The authors thank Lisa Coffey for growing plants for testing, Leland Harker for assistance in PCB design and manufacturing, Shawana Tabassum and Mehmet Oren for assistance in testing of sensors, and Dr. Kasthurirangan Gopalakrishnan, Dr. Sunghwan Kim, and Dr. Peter Taylor for helpful discussions. All the above names are affiliated with the Iowa State University, except for Mehmet Oren.

Conflict of Interest

The authors declare no conflict of interest.

Keywords

graphene, sensors, tapes, wearable electronics

Received: August 21, 2017
Revised: September 11, 2017
Published online: November 17, 2017

[1] A. R. Madaria, A. Kumar, F. N. Ishikawa, C. Zhou, *Nano Res.* **2010**, *3*, 564.
[2] F. E. Wiria, C. L. Tham, A. S. Subramanian, J. N. Tey, X. Qi, C. K. Cheng, B. Salam, *J. Solid State Electrochem.* **2016**, *20*, 1895.
[3] H. Kizil, M. O. Pehlivaner, L. Trabzon, *Adv. Mater. Res.* **2014**, *970*, 132.
[4] C. Wang, J. Chien, K. Takei, T. Takahashi, J. Nah, A. M. Niknejad, A. Javey, *Nano Lett.* **2012**, *12*, 1527.
[5] Y. Wang, R. Yang, Z. Shi, L. Zhang, D. Shi, E. Wang, G. Zhang, *ACS Nano* **2011**, *5*, 3645.
[6] G. Schwartz, B. C.-K. Tee, J. Mei, A. L. Appleton, D. H. Kim, H. Wang, Z. Bao, *Nat. Commun.* **2013**, *4*, 1859.
[7] Y. Zheng, Z. He, Y. Gao, J. Liu, *Sci. Rep.* **2013**, *3*, 1786.
[8] F. N. Ishikawa, H.-K. Chang, K. Ryu, P.-C. Chen, A. Badmaev, L. G. De Arco, G. Shen, C. Zhou, *ACS Nano* **2009**, *3*, 73.

[9] Y.-H. Lee, J.-S. Kim, J. Noh, I. Lee, H. J. Kim, S. Choi, J. Seo, S. Jeon, T.-S. Kim, J.-Y. Lee, J. W. Choi, *Nano Lett.* **2013**, *13*, 5753.
[10] X. Pu, L. Li, H. Song, C. Du, Z. Zhao, C. Jiang, G. Cao, W. Hu, Z. L. Wang, *Adv. Mater.* **2015**, *27*, 2472.
[11] Y. H. Kim, S. J. Kim, Y.-J. Kim, Y.-S. Shim, S. Y. Kim, B. H. Hong, H. W. Jang, *ACS Nano* **2015**, *9*, 10453.
[12] G. Lu, S. Park, K. Yu, R. S. Ruoff, L. E. Ocola, D. Rosenmann, J. Chen, *ACS Nano* **2011**, *5*, 1154.
[13] H. G. Sudibya, Q. He, H. Zhang, P. Chen, *ACS Nano* **2011**, *5*, 1990.
[14] S. J. Park, O. S. Kwon, S. H. Lee, H. S. Song, T. H. Park, J. Jang, *Nano Lett.* **2012**, *12*, 5082.
[15] P. Labroo, Y. Cui, *Biosens. Bioelectron.* **2013**, *41*, 852.
[16] Y. Pang, H. Tian, L. Tao, Y. Li, X. Wang, N. Deng, Y. Yang, T.-L. Ren, *ACS Appl. Mater. Interfaces* **2016**, *8*, 26458.
[17] S. Chun, Y. Kim, H. Jin, E. Choi, S.-B. Lee, W. Park, *Carbon* **2014**, *78*, 601.
[18] K. K. Sadasivuni, A. Kafy, L. Zhai, H.-U. Ko, S. Mun, J. Kim, *Small* **2015**, *11*, 994.
[19] S. Lee, A. Reuveny, J. Reeder, S. Lee, H. Jin, Q. Liu, T. Yokota, T. Sekitani, T. Isoyama, Y. Abe, Z. Suo, T. Someya, *Nat. Nanotechnol.* **2016**, *11*, 472.
[20] M. S. Romano, N. Li, D. Antiohos, J. M. Razal, A. Nattestad, S. Beirne, S. Fang, Y. Chen, R. Jalili, G. G. Wallace, R. Baughman, J. Chen, *Adv. Mater.* **2013**, *25*, 6602.
[21] S. Han, D. Wu, S. Li, F. Zhang, X. Feng, *Adv. Mater.* **2014**, *26*, 849.
[22] M. Ali, W. Hong, S. Oren, Q. Wang, Y. Wang, H. Jiang, L. Dong, *RSC Adv.* **2016**, *6*, 67184.
[23] Q. Wang, W. Hong, L. Dong, *Nanoscale* **2016**, *8*, 7663.
[24] M. Ali, K. Mondal, Y. Jiao, S. Oren, Z. Xu, A. Sharma, L. Dong, *ACS Appl. Mater. Interfaces* **2016**, *8*, 20570.
[25] K. I. Bolotin, K. J. Sikes, Z. Jiang, M. Klima, G. Fudenberg, J. Hone, P. Kim, H. L. Stormer, *Solid State Commun.* **2008**, *146*, 351.
[26] K. Xu, K. Wang, W. Zhao, W. Bao, E. Liu, Y. Ren, M. Wang, Y. Fu, J. Zeng, Z. Li, W. Zhou, F. Song, X. Wang, Y. Shi, X. Wan, M. S. Fuhrer, B. Wang, Z. Qiao, F. Miao, D. Xing, *Nat. Commun.* **2015**, *6*, 8119.
[27] C. Lee, X. Wei, J. W. Kysar, J. Hone, *Science* **2008**, *321*, 385.
[28] B. An, Y. Ma, W. Li, M. Su, F. Li, Y. Song, *Chem. Commun.* **2016**, *52*, 10948.
[29] M. S. Mannoor, H. Tao, J. D. Clayton, A. Sengupta, D. L. Kaplan, R. R. Naik, N. Verma, F. G. Omenetto, M. C. McAlpine, *Nat. Commun.* **2012**, *3*, 763.
[30] Y. Jiao, C. W. Young, S. Yang, S. Oren, H. Ceylan, S. Kim, K. Gopalakrishnan, P. C. Taylor, L. Dong, *IEEE Sens. J.* **2016**, *16*, 7870.
[31] M. Amjadi, K.-U. Kyung, I. Park, M. Sitti, *Adv. Funct. Mater.* **2016**, *26*, 1678.
[32] T. Yang, W. Wang, H. Zhang, X. Li, J. Shi, Y. He, Q.-S. Zheng, Z. Li, H. Zhu, *ACS Nano* **2015**, *9*, 10867.
[33] J. W. Park, J. Jang, *Carbon* **2015**, *87*, 275.
[34] T. T. Tung, M. Castro, T. Y. Kim, K. S. Suh, J.-F. Feller, *J. Mater. Chem.* **2012**, *22*, 21754.
[35] C. Hou, H. Wang, Q. Zhang, Y. Li, M. Zhu, *Adv. Mater.* **2014**, *26*, 5018.
[36] D. H. Ho, Q. Sun, S. Y. Kim, J. T. Han, D. H. Kim, J. H. Cho, *Adv. Mater.* **2016**, *28*, 2601.
[37] C. Wu, J. Feng, L. Peng, Y. Ni, H. Liang, L. He, Y. Xie, *J. Mater. Chem.* **2011**, *21*, 18584.
[38] K. S. Novoselov, A. K. Geim, S. V. Morozov, D. Jiang, Y. Zhang, S. V. Dubonos, I. V. Grigorieva, A. A. Firsov, *Science* **2004**, *306*, 666.
[39] L. Wang, J. Yu, Y. Zhang, H. Yang, L. Miao, Y. Song, *ACS Appl. Mater. Interfaces* **2017**, *9*, 9089.
[40] F. Tehrani, L. Reiner, B. Bavarian, *PLoS One* **2015**, *10*, e0145036.
[41] B. Alemán, W. Regan, S. Aloni, V. Altoe, N. Alem, C. Girit, B. Geng, L. Maserati, M. Crommie, F. Wang, A. Zettl, *ACS Nano* **2010**, *4*, 4762.
[42] L. Zhang, S. Diao, Y. Nie, K. Yan, N. Liu, B. Dai, Q. Xie, A. Reina, J. Kong, Z. Liu, *J. Am. Chem. Soc.* **2011**, *133*, 2706.
[43] Z. Sun, C. L. Pint, D. C. Marcano, C. Zhang, J. Yao, G. Ruan, Z. Yan, Y. Zhu, R. H. Hauge, J. M. Tour, *Nat. Commun.* **2011**, *2*, 559.
[44] D. Kuzum, H. Takano, E. Shim, J. C. Reed, H. Juul, A. G. Richardson, J. De Vries, H. Bink, M. A. Dichter, T. H. Lucas, D. A. Coulter, E. Cubukcu, B. Litt, *Nat. Commun.* **2014**, *5*, 5259.
[45] S.-H. Bae, Y. Lee, B. K. Sharma, H.-J. Lee, J.-H. Kim, J.-H. Ahn, *Carbon* **2013**, *51*, 236.
[46] X. Li, W. Cai, J. An, S. Kim, J. Nah, D. Yang, R. Piner, A. Velamakanni, I. Jung, E. Tutuc, S. K. Banerjee, L. Colombo, R. S. Ruoff, *Science* **2009**, *324*, 1312.
[47] A. M. H. Ng, Y. Wang, W. C. Lee, L. C. Teck, K. P. Loh, H. Y. Low, *Carbon* **2014**, *67*, 390.
[48] K. Yong, A. Ashraf, P. Kang, S. Nam, *Sci. Rep.* **2016**, *6*, 24890.
[49] M. Hofmann, Y.-P. Hsieh, A. L. Hsu, J. Kong, *Nanoscale* **2014**, *6*, 289.
[50] M. F. El-Kady, R. B. Kaner, *Nat. Commun.* **2013**, *4*, 1475.
[51] B. Senyuk, N. Behabtu, A. Martinez, T. Lee, D. E. Tsentalovich, G. Ceriotti, J. M. Tour, M. Pasquali, I. I. Smalyukh, *Nat. Commun.* **2015**, *6*, 7157.
[52] J. Lin, Z. Peng, Y. Liu, F. Ruiz-Zepeda, R. Ye, E. L. G. Samuel, M. J. Yacaman, B. I. Yakobson, J. M. Tour, *Nat. Commun.* **2014**, *5*, 5714.
[53] H. Tian, Y. Shu, Y.-L. Cui, W.-T. Mi, Y. Yang, D. Xie, T.-L. Ren, *Nanoscale* **2014**, *6*, 699.
[54] H. Tian, Y. Shu, X.-F. Wang, M. A. Mohammad, Z. Bie, Q.-Y. Xie, C. Li, W.-T. Mi, Y. Yang, T.-L. Ren, *Sci. Rep.* **2015**, *5*, 8603.
[55] S. R. Das, Q. Nian, A. A. Cargill, J. A. Hondred, S. Ding, M. Saei, G. J. Cheng, J. C. Claussen, *Nanoscale* **2016**, *8*, 15870.
[56] J. S. Lee, N. H. Kim, M. S. Kang, H. Yu, D. R. Lee, J. H. Oh, S. T. Chang, J. H. Cho, *Small* **2013**, *9*, 2817.
[57] Q. He, H. G. Sudibya, Z. Yin, S. Wu, H. Li, F. Boey, W. Huang, P. Chen, H. Zhang, *ACS Nano* **2010**, *4*, 3201.
[58] W. Zheng, in *Polymer Thin Films* (Ed: A. A. Hashim), InTech, Rijeka, Croatia **2010**, Ch. 10.
[59] S. Ebnesajjad, C. Ebnesajjad, *Surface Treatment of Materials for Adhesion Bonding*, 2nd ed., William Andrew Publishing, Norwich, NY, USA **2014**, Ch. 5.
[60] H. Kim, B. Yoon, J. Sung, D.-G. Choi, C. Park, *J. Mater. Chem.* **2008**, *18*, 3489.
[61] W.-W. Liu, B.-Y. Xia, X.-X. Wang, J.-N. Wang, *Front. Mater. Sci.* **2012**, *6*, 176.
[62] Dupont Kapton Summary of Properties, https://www.dupont.com/content/dam/dupont/products-and-services/membranes-and-films/polyimde-films/documents/DEC-Kapton-summary-of-properties.pdf (accessed: March 2017).
[63] I.-Y. Jeon, H.-J. Choi, M. J. Ju, I. T. Choi, K. Lim, J. Ko, H. K. Kim, J. C. Kim, J.-J. Lee, D. Shin, S.-M. Jung, J.-M. Seo, M.-J. Kim, N. Park, L. Dai, J.-B. Baek, *Sci. Rep.* **2013**, *3*, 2260.
[64] X. Feng, Y. Zhang, J. Zhou, Y. Li, S. Chen, L. Zhang, Y. Ma, L. Wang, X. Yan, *Nanoscale* **2015**, *7*, 2427.
[65] Y. R. Jeong, H. Park, S. W. Jin, S. Y. Hong, S.-S. Lee, J. S. Ha, *Adv. Funct. Mater.* **2015**, *25*, 4228.
[66] 3M™ Electrically Conductive Adhesive Transfer Tape 9707, https://multimedia.3m.com/mws/media/536957O/3mtm-electrically-conductive-adhesive-transfer-tape-9707.pdf (accessed: May 2014).
[67] P. S. Schnable, D. Ware, R. S. Fulton, J. C. Stein, F. Wei, S. Pasternak, C. Liang, J. Zhang, L. Fulton, T. A. Graves, P. Minx, A. D. Reily, L. Courtney, S. S. Kruchowski, C. Tomlinson, C. Strong, K. Delehaunty, C. Fronick, B. Courtney, S. M. Rock, E. Belter, F. Y. Du, K. Kim, R. M. Abbott, M. Cotton, A. Levy, P. Marchetto, K. Ochoa, S. M. Jackson, B. Gillam, W. Chen, L. Yan, J. Higginbotham, M. Cardenas, J. Waligorski, E. Applebaum, L. Phelps, J. Falcone, K. Kanchi, T. Thane, A. Scimone, N. Thane, J. Henke, T. Wang, J. Ruppert, N. Shah, K. Rotter, J. Hodges, E. Ingenthron, M. Cordes,

S. Kohlberg, J. Sgro, B. Delgado, K. Mead, A. Chinwalla, S. Leonard, K. Crouse, K. Collura, D. Kudrna, J. Currie, R. F. He, A. Angelova, S. Rajasekar, T. Mueller, R. Lomeli, G. Scara, A. Ko, K. Delaney, M. Wissotski, G. Lopez, D. Campos, M. Braidotti, E. Ashley, W. Golser, H. Kim, S. Lee, J. K. Lin, Z. Dujmic, W. Kim, J. Talag, A. Zuccolo, C. Fan, A. Sebastian, M. Kramer, L. Spiegel, L. Nascimento, T. Zutavern, B. Miller, C. Ambroise, S. Muller, W. Spooner, A. Narechania, L.Y. Ren, S. Wei, S. Kumari, B. Faga, M. J. Levy, L. McMahan, P. Van Buren, M. W. Vaughn, K. Ying, C. T. Yeh, S. J. Emrich, Y. Jia, A. Kalyanaraman, A. P. Hsia, W. B. Barbazuk, R. S. Baucom, T. P. Brutnell, N. C. Carpita, C. Chaparro, J. M. Chia, J. M. Deragon, J. C. Estill, Y. Fu, J. A. Jeddeloh, Y. J. Han, H. Lee, P. Li, D. R. Lisch, S. Liu, Z. Liu, D. H. Nagel, M. C. McCann, P. SanMiguel, A. M. Myers, D. Nettleton, J. Nguyen, B. W. Penning, L. Ponnala, K. L. Schneider, D. C. Schwartz, A. Sharma, C. Soderlund, N. M. Springer, Q. Sun, H. Wang, M. Waterman, R. Westerman, T. K. Wolfgruber, L. Yang, Y. Yu, L. Zhang, S. Zhou, Q. Zhu, J. L. Bennetzen, R. K. Dawe, J. Jiang, N. Jiang, G. G. Presting, S. R. Wessler, S. Aluru, R. A. Martienssen, S. W. Clifton, W. R. McCombie, R. A. Wing, R. K. Wilson, *Science* **2009**, *326*, 1112.

[68] A. Kozbial, Z. Li, C. Conaway, R. McGinley, S. Dhingra, V. Vahdat, F. Zhou, B. D'Urso, H. Liu, L. Li, *Langmuir* **2014**, *30*, 8598.

[69] X. D. Huang, S. M. Bhangale, P. M. Moran, N. L. Yakovlev, J. Pan, *Polym. Int.* **2003**, *52*, 1064.

[70] Accu Dyne Test, https://www.accudynetest.com/polytable_02.html (accessed: April 2017).

[71] Graphene Supermarket, https://graphene-supermarket.com/Conductive-Graphene-Dispersion-100.html (accessed: January 2017).

